J Mater Sci (2018) 53:1014–1023

Ceramics

Enhanced magnetoelectric coupling in La-modified $Bi_5Co_{0.5}Fe_{0.5}Ti_3O_{15}$ multiferroic ceramics

Sheng Liu[1], Shuoqing Yan[1], Heng Luo[1], Lingling Yao[1], Zhaowen Hu[1], Shengxiang Huang[1], and Lianwen Deng[1,*]

[1] School of Physics and Electronics, Institute of Super-Microstructure and Ultrafast Process in Advanced Materials, Central South University, Changsha 410083, China

Received: 2 August 2017
Accepted: 18 September 2017
Published online: 22 September 2017

ABSTRACT

Multiferroic properties of La-modified four-layered perovskite $Bi_{5-x}La_xFe_{0.5}Co_{0.5}Ti_3O_{15}$ ($0 \le x \le 1$) ceramics were investigated, by analyzing the magnetodielectric effect, magneto-polarization response and magnetoelectric conversion. X-ray diffraction indicated the formation of pure Aurivillius ceramics, and Raman spectroscopy revealed the Bi ions displacement and the crystal structure variation. The enhancement of ferromagnetic and ferroelectric properties was observed in $Bi_{5-x}La_xFe_{0.5}Co_{0.5}Ti_3O_{15}$ after La modification. The evidence for enhanced ME coupling was determined by magnetic field-induced marked variations in the dielectric constant and polarization. A maximum ME coefficient of 1.15 mV/cm·Oe was achieved in $Bi_{4.25}La_{0.75}Fe_{0.5}Co_{0.5}Ti_3O_{15}$ ceramic, which provides the possible promise for novel magnetoelectric device application.

Introduction

Multiferroic magnetoelectrics, coupling between electric and magnetic orderings, offer a wide scope of potential applications and an excellent abundance with fundamental physics [1–3]. The interplay between ferroelectricity and magnetism, namely magnetoelectric (ME) effect, allows an additional degree of freedom in multifunction device designing, which make devices more attractive than the use of ferroelectricity or magnetism only [4–6]. Much of the pioneering works on multiferroics have been devoted to introduce these two order parameters in a single-phase material. For example, the observations of electric field-induced spin flop in $BiFeO_3$ [7], magnetic controlled ferroelectric polarization in $La_3Ni_2NbO_9$ [8] and spin-assisted ferroelectricity in $CaBaCo_4O_7$ [9] were attractive from the fundamental and technical perspectives. However, the single-phase multiferroics above room temperature (RT) are rare in nature and exhibit weak ME coupling, originating from the mutual exclusion of ferroelectricity and ferromagnetism in d_0 electronic structure for the B-site elements [2–4]. So continuing effort to search for single phase with high ME amplitude and sensitivity above RT should be undertaken. Several approaches of searching for desirable single-phase multiferroics with ferroelectrically and magnetically

Address correspondence to E-mail: denglw@csu.edu.cn

DOI 10.1007/s10853-017-1604-6

combined compound at atomic scale have been addressed, which include superlattices and layer-structured materials, e.g., the bismuth-based layered compound.

Layered bismuth titanates with Aurivillius structure, which can be viewed as inserting the unit of $BiFeO_3$ into the three-layered $[Bi_2Ti_3O_{10}]^{2-}$ perovskite slabs of the parental $Bi_4Ti_3O_{12}$ ferroelectrics ($n BiFeO_3 \cdot Bi_4Ti_3O_{12}$), is interesting compounds with the possible ME coupling at RT [10–13]. By incorporating a magnetic unit into a ferroelectric $Bi_4Ti_3O_{12}$ block, magnetic properties are enhanced by the coupling between magnetic ions, such as Fe^{3+}, Ni^{2+} and Co^{3+} [13–15]. More importantly, partially replacing Bi ions by rare earth ions with *d*-block electronic configuration ions, such as La^{3+}, and with *f*-block ions, such as Nd^{3+} and Sm^{3+}, further remarkably improve the ferroelectric polarization, ferromagnetic property and magnetodielectric (MD) effect [16–18]. Such rare earth ions substitution approach in Aurivillius structure was mainly demonstrated in four-layer $Bi_5FeTi_3O_{15}$ ceramics, composed by inserting one mole $BiFeO_3$ into one mole $Bi_4Ti_3O_{12}$ [15–19]. Yang et al. found that the Nd-modified $Bi_5Fe_{0.7}Co_{0.3}Ti_3O_{15}$ ceramic presents a large ferromagnetism with $2M_r = 330$ memu/g and an enhanced MD response of 0.12% at RT [18, 19]. Recently, Mao et al. [15] realized the enhancement of ferromagnetism and MD effect in $Bi_5Fe_{0.5}Co_{0.3}Ti_3O_{15}$ ceramic by the La substitution, and the observed MD value of $Bi_{4.25}La_{0.75}Fe_{0.5}Co_{0.5}Ti_3O_{15}$ reached up to 8.1% under the magnetic field of 1 T. Although several studies have reported on the ferroelectric, ferromagnetic and MD properties in doped four-layer Aurivillius, little attention is focused on the magnetic field dependence of the ferroelectric polarization and ME output. It is expected that such studies will help in further elucidating the ME response in four-layer Aurivillius family in fact. To our knowledge, the ions doping level is crucial for improving ME properties and designing a new class of multiferroics. In this work, we prepared La-doped four-layer Aurivillius $Bi_{5-x}La_xTi_3Fe_{0.5}Co_{0.5}O_{15}$ ($0 \le x \le 1$) system with different doping content, and then systemically investigated the structural, ferroelectric, magnetic properties and ME coupling. The ME coupling is characterized by the MD response, magneto-polarization property and ME voltage sensitivity. Excitingly, the La-substituted ceramics exhibits a significant enhancement in the ME coupling at RT, especially for the $Bi_{4.25}La_{0.75}Fe_{0.5}Co_{0.5}Ti_3O_{15}$ ceramic.

Experimental

$Bi_{5-x}La_xTi_3Fe_{0.5}Co_{0.5}O_{15}$ ($0 \le x \le 1$) ceramics were synthesized by a modified sol–gel method. The process involves two steps. Firstly, the parental powders of $Bi_{4-x}La_xTi_3O_{12}$ ($0 \le x \le 1$) were synthesized by the citrate combustion method. Analytical reagent grade $Ti[OCH(CH_3)_2]_4$, $Bi(NO_3)_3{\cdot}5H_2O$ (5 wt% excess to compensate the volatilization of Bi) and $La(NO_3)_3{\cdot}6H_2O$ were dissolved into the citric acid solution with glycol in stoichiometry. Ammonia was added into the mixed solutions to regulate PH to 7. Then the precursor solution was evaporated at 90 °C and dried at 120 °C to obtain the xerogel. After that, the xerogel was pre-sintered at 450 °C for 4 h and sintered at 750 °C for 4 h to obtain $Bi_{4-x}La_xTi_3O_{12}$ powders. Secondly, the as-obtained $Bi_{4-x}La_xTi_3O_{12}$ powders were soaked in $BiFe_{0.5}Co_{0.5}O_3$ precursor solution with mole ratio of 1:1, which was taken in stoichiometric amounts using $Bi(NO_3)_3{\cdot}5H_2O$, $Fe(NO_3)_3{\cdot}9H_2O$, $Co(NO_3)_2{\cdot}6H_2O$ and citric acid solution. This powder-in-sol precursor hybrid processing allows for a high purification and densification, a uniform dispersion and low-temperature sintering feature. The resultant solution was then subjected to heat at 90 °C with continuous stirring for 4–5 h and dried at 120 °C to obtain the xerogel. Afterward, the xerogel was pre-sintered at 450 °C for 4 h to burn out the organic species. The pre-sintered powders were ground, pelleted and finally sintered at 840 °C for 4 h in air. The sintered pellets were electroded using silver paint on both the surfaces to carry out subsequently electrical and ME measurement.

The phase identification and micromorphology of sintered pellets were characterized using X-ray diffraction (XRD, Philips X-pert PRO) and scanning electron microscope (SEM, TESCAN VEGA 3), respectively. The Raman mode was recorded with Raman spectrometer system (BWS435, B & WTEK). The grain size of the ceramic samples was determined by the mean linear intercept, and the bulk density of pellets was measured using Archimedes' method. Magnetic hysteresis loops were studied by a vibrating samples magnetometer (VSM, Lakeshore 7404). Dielectric characteristics performed by combining a HP4284 LCR meter. Bulk density of pellets was performed using Archimedes' method. DC resistivity was measured using precision LCR meter (TH2829C). The effect of magnetic field on the

ferroelectric properties was evaluated by a ferroelectric tester based on Sawyer–Tower circuit. The magnetic field source for MD and ferroelectric properties measurement is used a custom designed magnet, and magnetic field direction is parallel to the surface of the pellet. The ME measurement were taken using the lock-in technique. A small alternating magnetic field H ($f = 1$ kHz, $H_{ac} = 1.0$ Oe) was generated using a solenoid that was superimposed onto a magnetic bias up to 3.5 kOe.

Result and discussion

Figure 1 displays the XRD patterns of $Bi_{5-x}La_xTi_3Fe_{0.5}Co_{0.5}O_{15}$ ($0 \le x \le 1$) ceramics. Inset shows the magnified XRD patterns in the vicinity of 29.5°–31°. All the XRD peaks agree with the four-layered perovskite Aurivillius structure, in accordance with the standard XRD spectrum (JCPD no. 38-1257). No impurity phases are detected, indicating the monophasic nature of these ceramics. From the inset of Fig. 1, the diffraction peak (119) shifts toward low angle with increasing La content. This shifting is related to the lattice structure distortion driven by the difference of introduced ionic radius. Detailed variations of lattice parameters (listed in Table 1) are evaluated from the Rietveld refinements, and the sample is indexed with the orthorhombic lattice of the space group *F*2*mm*. With increasing *x*, the lattice constant *a* decreases while the lattice constant *b*, the lattice constant *c* and the cell volume increase. We also estimate the orthorhombicity [$\delta = 2(a - b)/(a + b)$] for all samples. It can be clearly noticed that the orthorhombicity (δ) decreases continuously with increasing *x*. The variation of δ implies the relaxation of orthorhombic structure distortion [20, 21], which may affect the electric and magnetic properties.

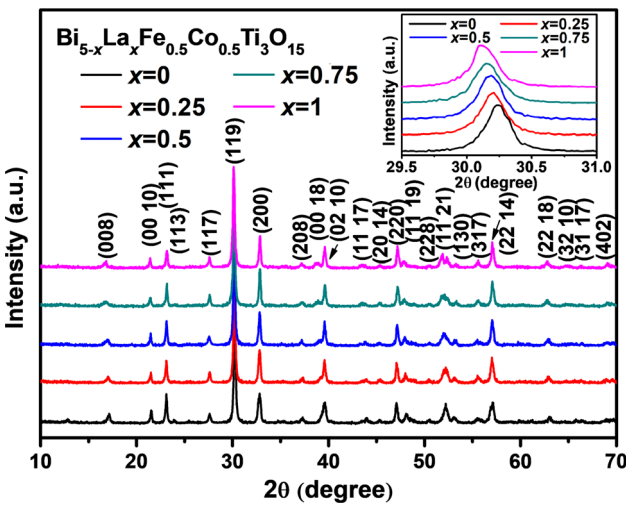

Figure 1 XRD patterns of $Bi_{5-x}La_xTi_3Fe_{0.5}Co_{0.5}O_{15}$ ($0 \le x \le 1$) ceramics. Inset shows the magnified XRD patterns in the vicinity of 29.5°–31°.

In order to understand the structural modification by substitution, the Raman spectra of $Bi_{5-x}La_xTi_3Fe_{0.5}Co_{0.5}O_{15}$ ($0 \le x \le 1$) ceramics are recorded and shown in Fig. 2. The observation of Raman modes at around 61, 89, 121, 154, 241, 264, 316, 469, 554, and 855 cm^{-1} confirmed the pure parental $Bi_4Ti_3O_{12}$ with orthorhombic structure [21, 22]. Based on the mass consideration of vibrational frequencies, the low-frequency Raman mode around 61 cm^{-1} is dominated by the displacement of Bi^{3+} ions in Bi_2O_2 layers and the triplet bands at 89, 121 and 154 cm^{-1} modes are assigned to the motion of Bi^{3+} ions (A-site) in the pseudo-perovskite slabs [23]. As shown in inset of Fig. 2, the mode at 61 cm^{-1} decreases slightly until $x = 0.75$ and then sharply drops with further increasing La content. The slight variation of this mode indicates the absence of La^{3+} ions participating the Bi_2O_2 layers in the substitution process with *x* below 0.75. Over this doping content, however, the sharp decrease implies that the introduced La^{3+} ions may partially occupy the Bi^{3+} in the Bi_2O_2 layers. For the triplet bands, the mode at 89 cm^{-1} softens continuously, while the modes at 121 and 154 cm^{-1} show a hardening tendency with increasing *x*. The evolution of the triplet bands mainly related to the A-site Bi^{3+} ions replaced by La^{3+} ions in the perovskite slab. Similar behaviors have been observed previously in La-modified $Bi_4Ti_3O_{12}$ [21] and Nd-modified $Bi_4Ti_3O_{12}$ [24] bismuth layer perovskites. The high-frequency internal modes above 200 cm^{-1} with A_{1g} character are related to the TiO_6 octahedron. The main modes at 264 and 855 cm^{-1} show the peak broadening and reduction in the intensity with increasing *x*, indicating the tilting of TiO_6 octahedron. This observation confirms the increase in *c*-parameter with increasing La content [25]. Since the appearance of splitting modes at 241 and 554 cm^{-1} in $Bi_4Ti_3O_{12}$ is Raman inactive according to the O_h symmetry of TiO_6, it often reflects the distortion of orthorhombic structure [20]. The suppression of these two modes with increasing La substitution in Raman spectra indicates the relaxation in distortion of TiO_6

Table 1 Rietveld refined lattice parameters of $Bi_{5-x}La_xTi_3Fe_{0.5}Co_{0.5}O_{15}$ ($0 \le x \le 1$) ceramics

Parameters	$Bi_{5-x}La_xTi_3Fe_{0.5}Co_{0.5}O_{15}$				
	$x = 0$	$x = 0.25$	$x = 0.5$	$x = 0.75$	$x = 1.0$
Space group	*F2mm*	*F2mm*	*F2mm*	*F2mm*	*F2mm*
a (Å)	5.460	5.455	5.451	5.443	5.437
b (Å)	5.421	5.424	5.428	5.432	5.434
c (Å)	41.16	41.21	41.33	41.46	41.52
Volume (Å^3)	1218.28	1219.32	1222.87	1226.05	1226.91
Orthorhombicity (δ)	7.17×10^{-3}	5.69×10^{-3}	4.22×10^{-3}	2.02×10^{-3}	0.55×10^{-3}
R_p (%)	5.64	5.37	6.49	6.28	6.51
wR_p (%)	8.63	9.39	9.41	8.09	8.85
χ^2 (%)	1.51	1.83	1.89	2.13	2.08

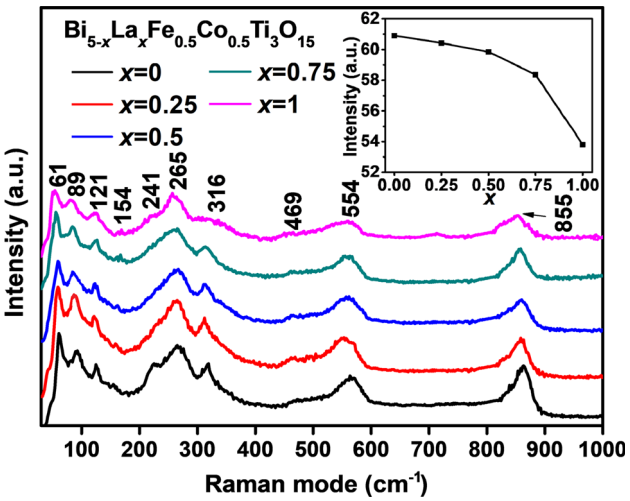

Figure 2 Raman spectra of $Bi_{5-x}La_xTi_3Fe_{0.5}Co_{0.5}O_{15}$ ($0 \le x \le 1$) ceramics in wavenumber ranging from 30 to 1000 cm^{-1} at RT. Inset shows the dependence of the low-frequency mode observed around 61 cm^{-1} on La doping content *x*.

octahedron and the decrease in orthorhombicity, which is in accordance with the result of XRD patterns.

The SEM images of the cross sections of $Bi_{5-x}La_xTi_3Fe_{0.5}Co_{0.5}O_{15}$ ($0 \le x \le 1$) ceramics are shown in Fig. 3. All ceramics have the plate-like grains, which are typical microstructural characteristic for Aurivillius bismuth layered compounds. The average size of plate-like grains decreases gradually from 3 to 1 μm with increasing La content. The low diffusion of La segregates at the grain boundaries and impedes the motion of grain boundaries during sintering, thus suppressing the grain growth [26]. On the other hand, the substitution of La ions for Bi also reduces the volatilization of Bi^{3+} and suppresses the formation of oxygen vacancies. The decrease in oxygen vacancies prevents the migration of ions between plate-like grains and then inhibits the grain growth. In addition, a few scattered micropores are observed, according to the relative density of ~ 90% (shown in Table 2) in the ceramics. The observed micropores were mainly located on the grain boundaries, relating to the random orientated and anisotropic plate-like grain growth.

Magnetic hysteresis loops of the $Bi_{5-x}La_xTi_3Fe_{0.5}Co_{0.5}O_{15}$ ($0 \le x \le 1$) ceramics measured at RT are shown in Fig. 4. The well-saturated magnetic hysteresis loops indicate the typical ferromagnetic ordering. For the La free sample, the remnant magnetization M_r and coercive field H_c is determined to be 35 memu/g and 291 Oe, respectively. With increasing La doping content, the M_r increases continuously and maximizes at $x = 1.0$ with the value of 131 memu/g, while the H_c decreases sharply with the $x \le 0.5$ and then increases slightly, shown in inset of Fig. 4. The improved ferromagnetism in the Co-substituted Aurivillius phase has been previously reported, mainly originating from the Dzyaloshinskii–Moriya (DM) interaction between Fe^{3+} and Co^{3+} through oxygen ions [12]. For the La-doped Aurivillius oxides, the further enhanced ferromagnetism is mainly attributed to the enhancement of Fe–O–Co clusters coupling. The 4*d* unoccupied orbits in La^{3+} ions partly accept the lone pairs of oxygen, leading to an intensively canted spin structure. This canted spin structure strengthens the coupling between the Fe-based and Co-based sublattices via the antisymmetric DM interaction. Moreover, the relaxed lattice distortion by the La^{3+} replacement for Bi^{3+} ions may release the locked latent magnetization and then contribute to the ferromagnetism interaction [27].

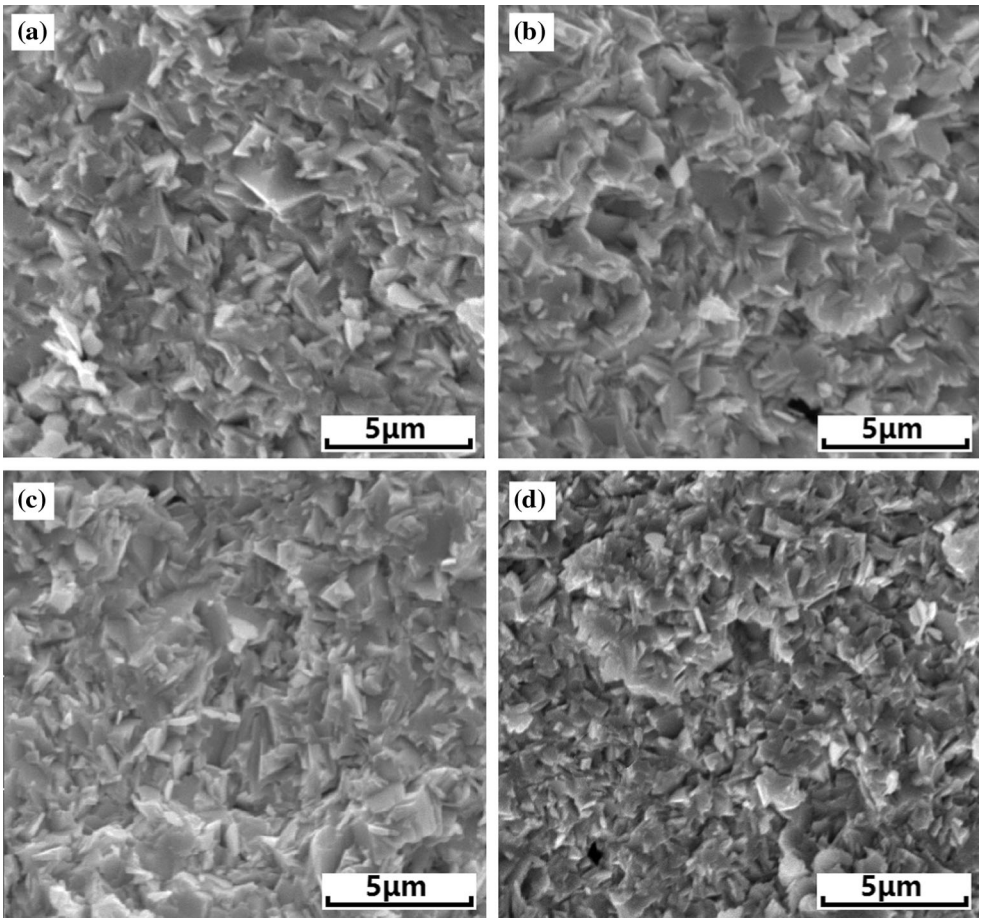

Figure 3 SEM morphology of the $Bi_{1-x}Nd_xFeO_3$ ceramics **a** $x = 0$, **b** $x = 0.25$, **c** $x = 0.75$ and **d** $x = 1$.

Table 2 Summary of the physical, ferroelectric, magnetic and ME parameters of the $Bi_{5-x}La_xTi_3Fe_{0.5}Co_{0.5}O_{15}$ ($0 \leq x \leq 1$) ceramics

La doping x	ρ (g/cm^3)	Relative density (%)	P_s (μC/cm^2)	P_r (μC/cm^2)	E_c (kV/cm)	M_s (memu/g)	M_r (memu/g)	H_c (Oe)	R_{dc} (Ω·cm)	α_{ME} (mV/cm·Oe)
0	7.227	89.88	1.82	1.6	33.54	194.2	35.2	291.1	9.55×10^8	0.67
0.25	7.271	90.43	2.29	2.5	37.06	334.4	53.5	112.7	1.33×10^9	0.87
0.50	7.299	90.33	2.78	2.9	37.23	608.9	82.7	66.3	1.58×10^9	0.99
0.75	7.269	89.96	4.35	4.45	37.25	779.2	112.6	68.5	2.42×10^9	1.15
1	7.321	90.15	3.82	3.94	38.24	870.5	131.2	70.7	1.53×10^9	1.03

Figure 5 exhibits the variation of dielectric constant ε' and loss tangent tanδ with frequency in $Bi_{5-x}La_xTi_3Fe_{0.5}Co_{0.5}O_{15}$ ($0 \leq x \leq 1$) ceramics. In the whole frequency range, the ε' decreases as increasing x from 0 to 0.75. In the layered bismuth titanates systems, it is inevitable that the volatilization of Bi existed in the structure during the sintering process. Many studies confirm this fact [12–15]. Due to the decrease in Bi in Bi–O structure, charge defects of oxygen vacancies are produced in the $Bi_5Ti_3Co_{0.5}Fe_{0.5}O_{15}$ ceramic. These defects along with $6s^2$ lone pair of Bi make a contribution to space-charge polarization under an external electric field. This is supported by the result of relatively strong dielectric dispersion in undoped sample, which shows a rapid decrease at low frequency (< 1 kHz) and remains constant at high frequency. The addition of La^{3+} reduces the formation of oxygen vacancies and restrains the space-charge

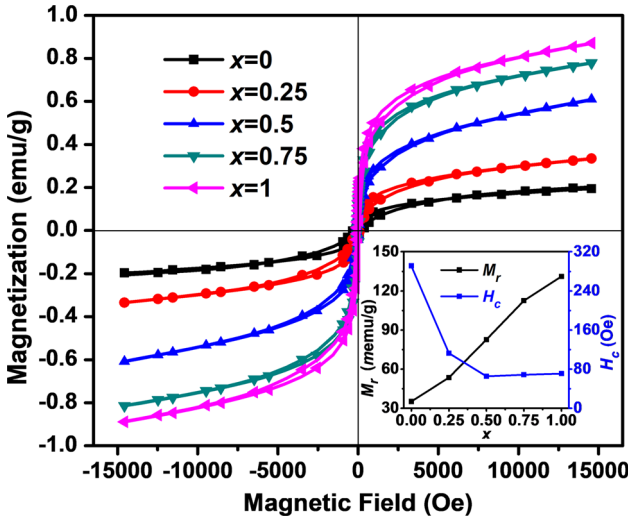

Figure 4 Magnetic hysteresis loops of $Bi_{5-x}La_xTi_3Fe_{0.5}Co_{0.5}O_{15}$ ($0 \le x \le 1$) ceramics with the inset of the magnified loops in low field.

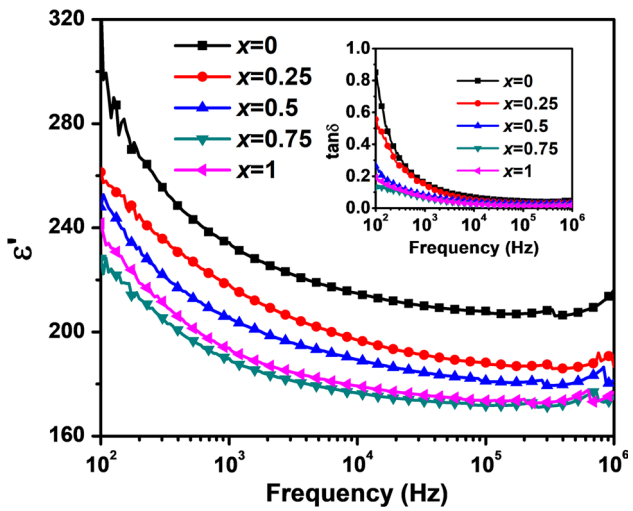

Figure 5 Variation of dielectric constant ε′ and dielectric loss tanδ with frequency for the $Bi_{5-x}La_xTi_3Fe_{0.5}Co_{0.5}O_{15}$ ($0 \le x \le 1$) ceramics.

polarization, leading to the decrease in ε′. Similar variation for the frequency dependence of tanδ is observed in inset of Fig. 5, where the tanδ of doped samples decreases significantly at low frequency as compared to the undoped $Bi_5Ti_3Fe_{0.5}Co_{0.5}O_{15}$ sample. However, in the high doping level of $x = 1$, a slight increase in ε′ can be found in $Bi_4LaTi_3Fe_{0.5}Co_{0.5}O_{15}$ ceramic. This is caused by the substitution of La^{3+} for Bi^{3+} at the $(Bi_2O_2)^{2+}$ layers. Bi_2O_2 layers act as both a reservoir for oxygen ions and an insulating layer to obstruct space charges hopping [28]. According to the analysis of Raman, the sharply decrease in the mode around 61 cm^{-1} at $x = 1$ indicates that the introduced La^{3+} ions partially occupy the Bi^{3+} in the Bi_2O_2 layers. The incorporation of La^{3+} ions into Bi_2O_2 layers destroys the original effects of the insulating layers as well as the space-charge compensation, which release oxygen vacancies and produce space charges. The increased space charges at grain boundaries contribute to interfacial polarization and lead to the increase in ε′.

Investigation over the magnetic-field-dependent dielectric properties, magnetodielectric (MD) effect, may give an understanding on ME coupling between the electric and the magnetic origins. MD effect is defined as $MD = 100\% \times [\varepsilon'(H) - \varepsilon'(0)]/\varepsilon'(0)$, where $\varepsilon'(H)$ and $\varepsilon'(0)$ are the ε′ at magnetic field and zero field, respectively. Figure 6a shows the frequency dependence of MD with the magnetic field of 0.8 T for $Bi_{5-x}La_xTi_3Fe_{0.5}Co_{0.5}O_{15}$ ($0 \le x \le 1$) ceramics. The MD of all ceramics experience continuous decrease with increasing frequency and the curves become flat at high frequency. The negative value of MD implies the decrease in ε′ at the applied magnetic field. The magnitude of MD increases with increasing magnetic field up to 0.8 T at 1 and 100 kHz, as shown in Fig. 6b. The maximum MD values reach up to 2.54% at 1 kHz and 1.18% at 100 kHz in $x = 0.75$. In layered Aurivillius structure, two major factors influence the MD response: the extrinsic effect, i.e., Maxwell–Wagner effect, and the intrinsic effect [29, 30], i.e., spin reorientation and structure distortion [31–33]. To see the influence of Maxwell–Wagner effect on the MD behavior, the dependence of tanδ on the magnetic field is measured and shown in inset of Fig. 6a, which is defined as $\Delta\tan\delta = 100\% \times [\tan\delta(H) - \tan\delta(0)]/\tan\delta(0)$; where $\tan\delta(H)$ and $\tan\delta(0)$ are the dielectric loss at magnetic field and zero field, respectively. Similarly, the Δtanδ presents negative value, suggesting the decreased tanδ in the presence of applied magnetic field. The decrease in the ε′ and tanδ at the applied magnetic field indicates that the dominant mechanism of the MD effect is not the extrinsic effect, i.e., Maxwell–Wagner effect. This phenomenon can be explained by the Maxwell–Wagner capacitor model, which shows the observed MD and Δtanδ present an opposite sign as function of the applied magnetic field [30]. In our case, the observed MD and Δtanδ exhibit the same sign (negative value) under the magnetic field. Therefore, the MD behavior is reasonably ascribed to the intrinsic effect: the incurred lattice distortion driven by the

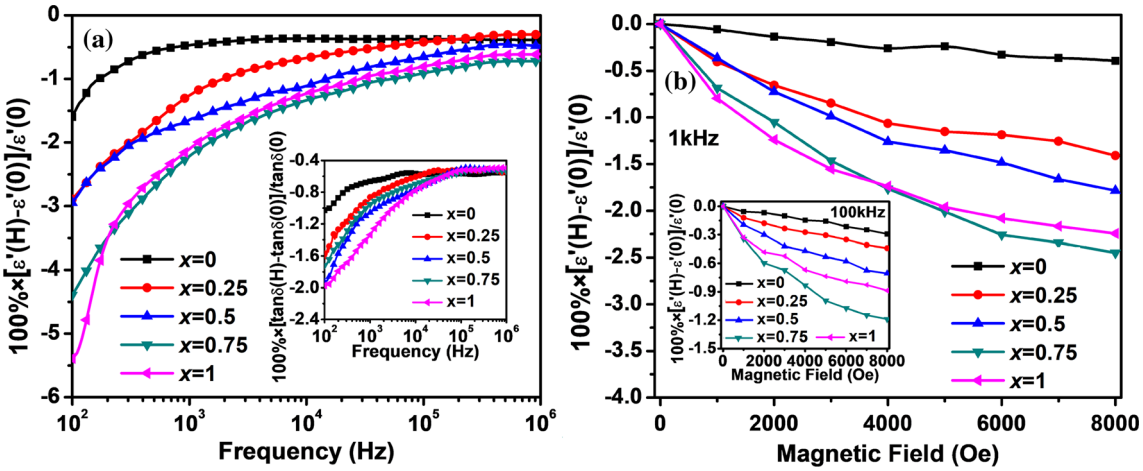

Figure 6 **a** Dependence of MD effect on frequency at the magnetic field of 0.8 T in $Bi_{5-x}La_xTi_3Fe_{0.5}Co_{0.5}O_{15}$ at RT. Inset shows the variation of tanδ on the magnetic field. **b** Variation of MD effect as a function of magnetic field at the frequency of 1 and 100 kHz (in inset).

La^{3+} substitution and the polarization response of Fe^{2+} and Fe^{3+} local dipoles induced by the spin reorientation under the magnetic field. In view of improved magnetic and MD properties in the high La modifying content for $Bi_{5-x}La_xTi_3Fe_{0.5}Co_{0.5}O_{15}$, the observations of the notable magneto-polarization and ME response are deserved.

Figure 7a shows the ferroelectric hysteresis loops of the $Bi_{5-x}La_xTi_3Fe_{0.5}Co_{0.5}O_{15}$ ($0 \le x \le 1$) measured at 1.5 kHz. The loops reflect clear ferroelectricity. Also, the loops exhibit less unsaturation under the electrical field of 70 kV/cm, and this result is different from the saturated loops measured at the high electrical field of 230 kV/cm in $Bi_5Ti_3Fe_{0.5}Co_{0.5}O_{15}$ system [11]. To exclude the effect of leakage-related contribution, the remanent polarization P_r dependence of frequency from 400 Hz to 2 kHz in undoped $Bi_5Ti_3Fe_{0.5}Co_{0.5}O_{15}$ ceramic was determined and is shown in inset Fig. 7a. The remnant polarization decreases rapidly from 400 Hz to 1.2 kHz, but keeps less change in the high-frequency region beyond 1.2 kHz. This indicates that the ferroelectricity is intrinsic nature (domain switching) and the leakage current is almost independent on the ferroelectric behavior in high-frequency region [27]. From Fig. 7b, the $2P_r$ increases sharply with increasing x, reaches the maximum at $x = 0.75$, and then decreases with further substitution. The largest $2P_r$ (4.45 $\mu C/cm^2$) is about 3 times larger than that of the undoped sample with $2P_r = 1.5$ $\mu C/cm^2$. This significant enhancement

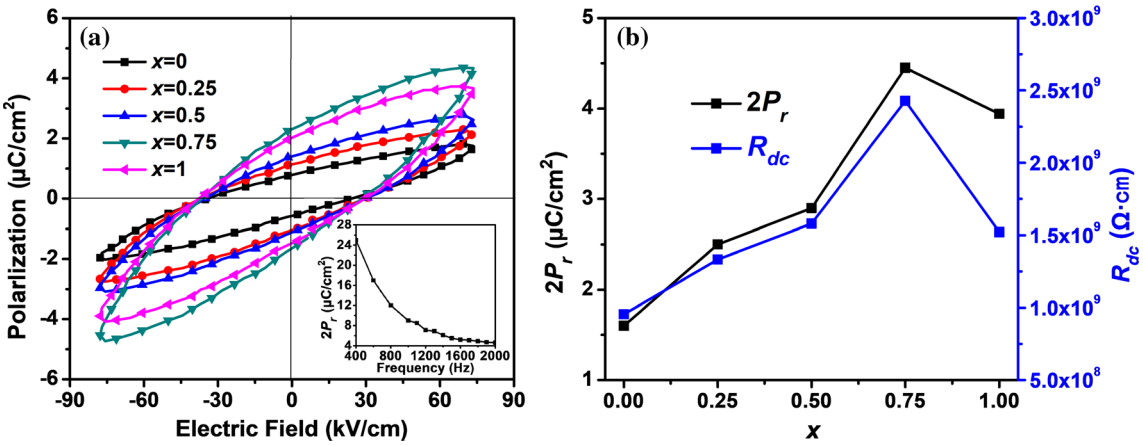

Figure 7 **a** Ferroelectric hysteresis loops of $Bi_{5-x}La_xTi_3Fe_{0.5}Co_{0.5}O_{15}$ ($0 \le x \le 1$) ceramics. Inset shows the dependence of the remanent polarization P_r in $Bi_5Ti_3Fe_{0.5}Co_{0.5}O_{15}$ on frequency from 400 Hz to 2 kHz. **b** Variation of $2P_r$ and resistivity R_{dc} as a function of La content.

of $2P_r$ on La doping may be attributed to non-centrosymmetic structure distortion and reduction in the oxygen vacancy concentration. By the occupation of La^{3+} ions at Bi^{3+} ions site in the perovskite slab, a lone s^2 pair of electrons of Bi^{3+} ion hybridization with an empty p orbital of Bi or O ion results in the non-centrosymmetic distortion of perovskite-like block and gives rise to the ferroelectric order [34]. On the other hand, the reduction oxygen vacancies tend to trap and weaken the segregation of vacancy at domain walls and speed up the polarization switching [35]. Over the doping content 0.75, the deterioration of $2P_r$ may arise from the induced leakage in ceramics. As discussed earlier, the incorporation of La^{3+} ions into Bi_2O_2 layers destroys the original effects of the insulating layers as well as the space-charge compensation and deteriorates the P_r. This can be further confirmed by the measured resistivity R_{dc} as shown in Fig. 7b. The R_{dc} presents a similar variation tendency to that found in $2P_r$.

In order to demonstrate the ME coupling aroused by La doping contribution, ferroelectric hysteresis loops of the $Bi_{5-x}La_xTi_3Fe_{0.5}Co_{0.5}O_{15}$ $(0 \le x \le 1)$ ceramics was performed under the magnetic field. Figure 8a shows the variation of remanent polarization ΔP_r and coercive field ΔE_c with x in $Bi_{5-x}La_xTi_3Fe_{0.5}Co_{0.5}O_{15}$ $(0 \le x \le 1)$ ceramics, which are defined as $\Delta P_r = P_r(H) - P_r(0)$ and $\Delta E_c = E_c(H) - E_c(0)$, where P_r(H), E_c(H) and P_r(0), E_c(0) are the polarization and coercive field measured with and without magnetic field at 0.8 T, respectively. The ΔP_r increases with increasing x and reaches a maximum value of 0.6 μC/cm^2 at $x = 0.75$. This increase trend is indicative of coupling between the two ordered ferroic parameters. In layered $Bi_{5-x}La_xTi_3Fe_{0.5}Co_{0.5}O_{15}$ structure, the weak magnetic moment by the measurement of magnetization indicates a canted antiferromagnetic ordering (spin structure). Such canted antiferromagnetic structure induces an electric polarization based on the DM interaction, which will be added to the ferroelectric polarization dominantly driven by Bi^{3+} ion displacement. The canted antiferromagnetism contributed to the polarization can be flipped by external magnetic field [13, 36]. By substituting La ions for Bi ions, the intensified canted spin structure and the enlarged ion displacement in Bi–O sublattice facilitate the ferroelectric polarization induced by inverse DM interaction under the magnetic field. Moreover, the enhanced polarization under the applied magnetic field partly arises from the strain coupling between the magnetic and ferroelectric domains. This can be confirmed by the changed coercive field ΔE_c shown in Fig. 8a. Due to the coupling between the magnetic and ferroelectric domains, the strain would induce a stress and then generate an additional electric field. This field orients the ferroelectric domains, causing a high pinning of domains [37, 38]. Consequently, a large coercive field is required to remove such additional aligning strength and switch more domains. At present, it is difficult to identify how the magnetic field will affect the polarization by current measurements, i.e., strain-mediated or DM interaction, or even both. Further research is required to elucidate this point. Figure 8b displays the variation of ME voltage coefficients α_{ME} with applied magnetic field

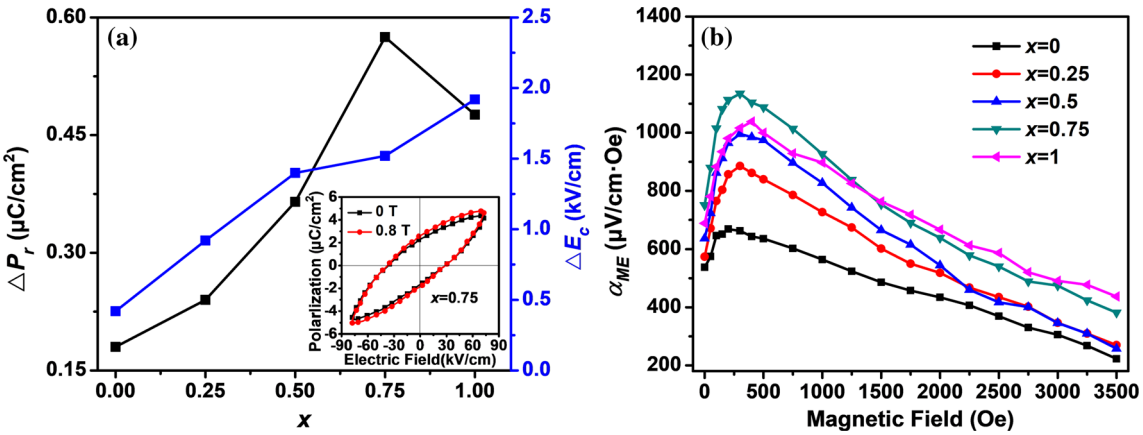

Figure 8 **a** Dependence of the changed remnant polarization ΔP_r on x without and with magnetic field of 0.8 T for the $Bi_{5-x}La_xTi_3Fe_{0.5}Co_{0.5}O_{15}$ $(0 \le x \le 1)$ ceramics at RT. Inset shows the ferroelectric hysteresis loops without and with magnetic field of 0.8 T for $x = 0.75$ sample. **b** Variation of ME voltage coefficients α_{ME} with magnetic field for the ceramics.

H at 1 kHz for $Bi_{5-x}La_xTi_3Fe_{0.5}Co_{0.5}O_{15}$ ($0 \le x \le 1$) ceramics. The coupling coefficient of all ceramics exhibits a non-monotonically ME behavior with increasing applied magnetic field and attain a peak value in the range of 200–400 Oe. The peak value of 1.15 mV/cm·Oe at $H = 300$ Oe is achieved for $x = 0.75$ sample, which is higher than that in the layered Aurivillius $Bi_5FeTi_3O_{15}$ (0.63 mV/cm·Oe at 300 Oe) ceramic [39], $Bi_{4-x}Sm_xTi_{3-x}Ni_xO_{12+\delta}$ ceramic (0.47 mV/cm·Oe at 300 Oe) [20] and $Bi_{4-x}Sm_xTi_{3-x}Co_xO_{12-\delta}$ ceramic (0.62 mV/cm·Oe at 300 Oe) [40]. Enhanced ME coupling was driven by La modification in four-layer Aurivillius ceramics, which will broaden the number of RT multiferroic candidates for ME multifunctional device application.

Conclusions

La-modified $Bi_{5-x}La_xTi_3Fe_{0.5}Co_{0.5}O_{15}$ ($0 \le x \le 1$) ceramics with enhanced ME coupling have been prepared by a modified sol–gel process. The XRD patterns and Rietveld refinement confirmed the formation of a pure Aurivillius ceramics, and Raman spectroscopy revealed the relaxation of orthorhombic distortion and the Bi displacements in the Bi_2O_2 layers. The La substitution was found to significantly improve the ferroelectric and magnetic properties of the $Bi_{5-x}La_xTi_3Fe_{0.5}Co_{0.5}O_{15}$ ceramics at RT. The enhanced ME coupling of the La-doped $Bi_{5-x}La_xTi_3Fe_{0.5}Co_{0.5}O_{15}$ ceramics was demonstrated by the large modulation of MD response, magneto-polarization behavior and direct ME output. The largest ME response was obtained in $Bi_{5-x}La_xTi_3Fe_{0.5}Co_{0.5}O_{15}$ ($x = 0.75$) with a MD value of 2.54%, magneto-polarization variation of 0.6 μC/cm^2 and ME conversion coefficient of 1.15 mV/cm·Oe, which may further encourage the potential use for four-layer Aurivillius ceramics in multifunctional ME device applications.

Acknowledgements

This work was supported by the National Key Research and Development Program of China (Grant No. 2017YFA0204600). The authors thank Dr. Jun Lu from Institute of Physics, CAS and Shichao Zhou from Junyutong corporation, for their kind help on magnetoelectric measurements.

References

[1] Nan CW, Bichurin MI, Dong S, Viehland D (2008) Multiferroic magnetoelectric composites: historical perspective, status, and future directions. J Appl Phys 103:031101

[2] Eerenstein W, Mathur ND, Scott JF (2006) Multiferroic and magnetoelectric materials. Nature (London) 442:759–765

[3] Dong S, Liu JM, Cheong SW, Ren Z (2015) Multiferroic materials and magnetoelectric physics: symmetry, entanglement, excitation, and topology. Adv Phys 64:519–626

[4] Hu JM, Chen LQ, Nan CW (2016) Multiferroic heterostructures integrating ferroelectric and magnetic materials. Adv Mater 28(1):15–39

[5] Sun NX, Srinivasan G (2012) Voltage control of magnetism in multiferroic heterostructures and devices. Spin 2:1240004

[6] Catalan G, Scott JF (2009) Physics and applications of bismuth ferrite. Adv Mater 21:2463–2485

[7] Schlom DG, Waghmare UV, Spaldin NA, Rabe KM, Wuttig M, Ramesh R (2003) Epitaxial $BiFeO_3$ multiferroic thin film heterostructures. Science 299(5613):1719–1722

[8] Singh K, Caignaert V, Chapon LC, Pralong V, Raveau B, Maignan A (2012) Gigantic magnetic-field-induced polarization and magnetoelectric coupling in a ferrimagnetic oxide $CaBaCo_4O_7$. Phys Rev B 86:024410

[9] Dey K, Indra A, De D, Majumdar S, Giri S (2016) Magnetoelectric coupling, ferroelectricity, and magnetic memory effect in double perovskite $La_3Ni_2NbO_9$. ACS Appl Mater Interfaces 8:12901–12907

[10] Kubel F, Schmid H (1992) X-ray room temperature structure from single crystal data, powder diffraction measurements and optical studies of the aurivillius phase $Bi_5(Ti_3Fe)O_{15}$. Ferroelectrics 129:101–112

[11] Mao X, Wang W, Chen X, Lu Y (2009) Multiferroic properties of layer-structured $Bi_5Fe_{0.5}Co_{0.5}Ti_3O_{15}$ ceramics. Appl Phys Lett 95:082901

[12] Dong XW, Wang KF, Wan JG, Zhu JS, Liu JM (2008) Magnetocapacitance of polycrystalline $Bi_5Ti_3FeO_{15}$ prepared by sol–gel method. J Appl Phys 103:094101

[13] Zhao H, Kimura H, Cheng Z, Osada M, Wang J, Wang X, Dou S, Liu Y, Yu J, Matsumoto T, Tohei T, Shibata N, Ikuhara Y (2014) Large magnetoelectric coupling in magnetically short-range ordered $Bi_5Ti_3FeO_{15}$ film. Sci Res 4:5255

[14] Chen XQ, Xiao J, Xue Y, Zeng XB, Yang FJ, Su P (2014) Room temperature multiferroic properties of Ni-doped Aurivillus phase $Bi_5Ti_3FeO_{15}$. Ceram Int 40:2635–2639

[15] Mao X, Sun H, Wang W, Chen X, Lu Y (2013) Ferromagnetic, ferroelectric properties, and magneto-dielectric effect of $Bi_{4.25}La_{0.75}Fe_{0.5}Co_{0.5}Ti_3O_{15}$ ceramics. Appl Phys Lett 102:072904

[16] Wu Y, Yao T, Lu Y, Zou B, Mao X, Huang FZ, Sun H, Chen XB (2017) Magnetic, dielectric, and magnetodielectric properties of Bi-layered perovskite $Bi_{4.25}Gd_{0.75}Fe_{0.5}Co_{0.5}Ti_3O_{15}$. J Mater Sci 52:7360–7368. doi:10.1007/s10853-017-0971-3

[17] Zuo XZ, Yang J, Song DP, Yuan B, Tang XW, Zhang KJ, Zhu XB, Song WH, Dai JM, Sun YP (2014) Magnetic, dielectric, and magneto-dielectric properties of rare-earth-substituted Aurivillius phase $Bi_6Fe_{1.4}Co_{0.6}Ti_3O_{18}$. J Appl Phys 116:154102

[18] Yang FJ, Su P, Wei C, Chen XQ, Yang CP, Cao WQ (2011) Large magnetic response in $(Bi_4Nd)Ti_3(Fe_{0.5}Co_{0.5})O_{15}$ ceramic at room-temperature. J Appl Phys 110:126102

[19] Chen XQ, Xue Y, Lu ZW, Xiao J, Yao J, Kang ZW, Su P, Yang FJ, Zeng XB, Sun HZ (2015) Magnetodielectric properties of $Bi_4NdTi_3Fe_{0.7}Co_{0.3}O_{15}$ multiferroic system. J Alloys Compd 622:288–291

[20] Paul J, Bhardwaj S, Sharma KK, Kotnala RK, Kumar R (2014) Room temperature multiferroic properties and magnetoelectric coupling in Sm and Ni substituted $Bi_{4-x}Sm_xTi_{3-x}Ni_xO_{12\pm\delta}$ ($x = 0$, 0.02, 0.05, 0.07) ceramics. J Appl Phys 115:204909

[21] Osada M, Tada M, Kakihana M, Watanabe T, Funakubo H (2001) Cation distribution and structural instability in $Bi_{4-x}La_xTi_3O_{12}$. Jpn J Appl Phys 40:5572–5575

[22] Kojima S, Shimada S (1996) Soft mode spectroscopy of bismuth titanate single crystals. Phys B Condens Matter 219:617–619

[23] Wang W, Gu SP, Mao XY, Chen XB (2007) Effect of Nd modification on electrical properties of mixed-layer Aurivillius phase $Bi_4Ti_3O_{12}$–$SrBi_4Ti_4O_{15}$. J Appl Phys 102:024102

[24] Liang K, Qia YJ, Lu CJ (2009) Temperature-dependent Raman scattering in ferroelectric $Bi_{4-x}Nd_xTi_3O_{12}$($x = 0$, 0.5, 0.85) single crystals. Raman Spectrosc 40:2088–2091

[25] Graves PR, Hua G, Myhra S, Thompson JG (1995) The Raman modes of the aurivillius phases: temperature and polarization dependence. J Solid State Chem 114:112–122

[26] Kumar S, Varma KBR (2009) Influence of lanthanum doping on the dielectric, ferroelectric and relaxor behaviour of barium bismuth titanate ceramics. J Phys D Appl Phys 42:075405

[27] Sun S, Wang G, Huang Y, Wang J, Peng R, Lu Y (2014) Structural transformation and multiferroic properties in Gd-doped $Bi_7Fe_3Ti_3O_{21}$ ceramics. RSC Adv 4:30440–30446

[28] Kim SK, Miyayama M, Yanagida H (1996) Electrical anisotropy and a plausible explanation for dielectric anomaly of $Bi_4Ti_3O_{12}$ single crystal. Mater Res Bull 31:121–131

[29] Padhan P, LeClair P, Gupta A, Srinivasan G (2008) Magnetodielectric response in epitaxial thin films of multiferroic Bi_2NiMnO_6. J Phys Condens Matter 20:355003

[30] Catalan G (2006) Magnetocapacitance without magnetoelectric coupling. Appl Phys Lett 88:102902

[31] Yamasaki Y, Kohara Y, Tokura Y (2009) Quantum magnetoelectric effect in iron garnet. Phys Rev B 80:140412

[32] Park BH, Kang BS, Bu SB, Noh TW, Lee J, Jo W (1999) Lanthanum-substituted bismuth titanate for use in non-volatile memories. Nature 401:682–684

[33] Sun H, Lu XM, Su J, Xu TT, Ju CC, Huang FZ, Zhu JS (2012) Multiferroic behaviour and the magneto-dielectric effect in $Bi_5FeTi_3O_{15}$ thin films. J Phys D Appl Phys 45:385001

[34] Liu S, Luo H, Yan SQ, Yao LL, He J, Li YH, He LH, Huang SX, Deng LW (2017) Effect of Nd-doping on structure and microwave electromagnetic properties of $BiFeO_3$. J Magn Magn Mater 426:267–272

[35] Scott JF, Araujo CAP (1989) Ferroelectric memories. Science 246:1400

[36] Kimura T, Goto T, Shintani H, Ishizaka K, Arima T, Tokura Y (2003) Magnetic control of ferroelectric polarization. Nature 426:55–58

[37] Palkar VR, Kundaliya DC, Malik SK, Bhattacharya S (2004) Magnetoelectricity at room temperature in the $Bi_{0.9-x}Tb_xLa_{0.1}FeO_3$ system. Phys Rev B 69:212102

[38] Kojima T, Sakai T, Watanabe T, Funakubo H, Saito K, Osada M (2002) Large remanent polarization of (Bi, Nd)$4Ti_3O_{12}$ epitaxial thin films grown by metalorganic chemical vapor deposition. Appl Phys Lett 80:2746–2748

[39] Singh RS, Bhimasankaram T, Kumar GS, Suryanarayana SV (1994) Dielectric and magnetoelectric properties of $Bi_5FeTi_3O_{15}$. Solid State Commun 91:567–569

[40] Paul J, Bhardwaj S, Sharma KK, Kotnala RK, Kumar R (2014) Room-temperature multiferroic properties and magnetoelectric coupling in $Bi_{4-x}Sm_xTi_{3-x}Co_xO_{12-\delta}$ ceramics. J Mater Sci 49:6056–6066. doi:10.1007/s10853-014-8328-7